Hindawi
International Journal of Aerospace Engineering
Volume 2022, Article ID 3641051, 13 pages
https://doi.org/10.1155/2022/3641051

Research Article

Vibration Behaviour Analysis and Vibration Suppression Studies of the Space Robot

Tian Yong,[1] **Yue Xiang**,[2,3] **Feng Yan**,[2] **and Jiang Binzhang**[2]

[1]*College of Mechanical Electrical and Vehicle Engineering, Weifang University, Weifang, China*
[2]*College of Engineering, Shenyang Agricultural University, Shenyang 110866, China*
[3]*State Key Laboratory of Robotics, Shenyang Institute of Automation, Chinese Academy of Sciences, Shenyang 110016, China*

Correspondence should be addressed to Yue Xiang; yuexiang@syau.edu.cn

Received 30 April 2022; Revised 12 June 2022; Accepted 21 August 2022; Published 9 September 2022

Academic Editor: Qing Gao

Aiming at the problem that the vibration of space robot will reduce the dynamic accuracy of robot, a method of vibration suppression of space robot through trajectory planning is proposed. First, the joint was simplified to a linear torsion spring, and the flexible rod was modelled using the finite element method, resulting in a flexible motion model of the robot. Then, a rigid-soft coupled dynamic model that combined the flexible motion model with the Lagrange method was established. Using the dynamic model, the factors influencing the vibration behaviour of space robots were analysed. Finally, the space robot was subjected to vibration suppression through trajectory planning. As verified by experimental analysis, different trajectories and loads affect the excitation force and inherent characteristics of the robot. In the design process, it is necessary to consider the relationship between the excitation force and natural frequency. The trajectory planning method has apparent effects on vibration suppression. The vibration amplitude was significantly reduced, which can improve the positioning accuracy and work efficiency of the robot.

1. Introduction

Space robots can be used to realise space control automation and intelligence, which can replace or assist astronauts in completing on-orbit assembly, on-orbit maintenance, fuel refuelling, orbit cleaning, spacecraft inspection, and other tasks, improve the efficiency of space exploration activities, and have broad application prospects. Space operation tasks, represented by on-orbit services, are becoming increasingly complex. Studying the precise and dexterous control technology of space robotic arms will be the key to human space exploration [1–5].

As an essential category of space robots, humanoid space robotic arms are mainly used to complete complex assembly, maintenance, and high-precision tasks. Compared with conventional robotic arms, space flexible robotic arms have the following characteristics: (1) the space robotic arm is made of lightweight materials, and the structure is a slender member, which is lightweight and fast in response; (2) the space manipulator develops in the direction of joint lightweight and integration, and adopts harmonic transmission, making the entire system a complex rigid-soft coupling nonlinear system [6]. Therefore, it is challenging to model the dynamics of spatially flexible robotic arms. Hu et al. presented an optimal configuration selection method for calibration of robots which is researched by the influencing factor separation method [7, 8]. When performing the grasping task, the space robot arm will inevitably generate vibrations owing to its flexibility, which will affect the accuracy of the operation. If the vibration is considerable, the entire system may fail. Therefore, to ensure that the space flexible robotic arm better serve space, an analysis of the vibration characteristics of the adjustable arm rod and the suppression of its vibration are necessary [9, 10].

There are three main methods for suppressing the low-frequency vibrations of flexible robots: passive control, active control, and trajectory planning. The effect of passive management is relatively simple; however, in practical applications, it can only be used for single linkages and components with relatively simple structures [11, 12]. The active control method

uses a controller design to monitor vibration and suppress vibration in real time [13]. Systematic dynamical equations were established using the conservation of linear momentum, conservation of angular momentum, theoretical modal methods, and Lagrange equations. For the fast subsystem, the speed difference feedback control and the linear secondary optimal control are designed to suppress the vibration of the flexible joint and flexible connecting rod, respectively [14]. The vibration suppression problem of flexible robots has been studied using optimal control methods. In these methods, the robot is suppressed by the dynamic model of the robot and state feedback equation [15].

The kinetic equations of the flexible robotic arm are decoupled using the singular perturbation method. Vibration is effectively suppressed by designing an observer to detect the vibration status of the system in real time, quickly predict the beat of the system, and control the robot system in real time through a feedback control system [16]. When the Kalman filter was used as the state trajectory quantity, the flex arm vibrated. A dynamic model of flexible manipulators considering hydrodynamic force was established by combining the Lagrange equation and Morison formula [17]. An adaptive fuzzy sliding mode control scheme to compensate for uncertain factors was designed to track the joint trajectory and suppress vibration. The rigid-soft coupling dynamics of a space robot system with flexible attachments were established. A vibration suppression method for autonomously capturing a target in the precollision stage of the base was proposed using a model prediction algorithm [18]. The finite-element method was used to establish a dynamic model of the system [19]. On this basis, vibration suppression experiments of six different cable-driven parallel robots were conducted using fuzzy PID control and active control methods. Active control methods place high demands on the accuracy of the dynamic models. Compared with operational management, trajectory planning has the advantages of low-accuracy requirements for dynamic models and relatively simple control. The method of trajectory planning is divided into two types: planning only at the kinematic level, such as planning the trajectory of the robot, taking the integral of the square of the acceleration as the optimization goal, reducing the impact, and reducing the vibration by smoothing the trajectory of the robot [20].

Using a five-time polynomial and the acceleration limit of each joint, a method of vibration suppression of a spatial flexible robotic arm based on trajectory planning that effectively suppresses the vibration of the robotic arm was proposed [21]. Planning at the kinematic level poorly affects the dampening vibrations and the other types of trajectory planning at the kinetic level. By establishing a flexible dynamic model of the robot, trajectory planning can be carried out based on spline curves and polynomial curves with the excitation force as the optimization goal; however, such a model is appropriate for single-degree-of-freedom or planar robots [22–25]. A vision-based noncontact vibration suppression method was proposed based on the vibration amplitude error prediction model, and an error estimation controller was designed so that the vibration could be controlled in real time [26]. However, this study only focused on vibration suppression, and the factors influencing the vibration behaviour were not revealed.

By analysing the influence of the motion law of triangles and trapezoids on the vibration of the system, it has been revealed that the residual vibration of the system is suppressed well when the deceleration time of the system is equal to the first-order vibration cycle of the system [27]. Zhao [28] responded to the dynamic response of a flexible robotic arm with a moving end effector in different motion states and analysed the effect of actuator movement on the robot vibration. Yu et al. [29, 30] proposed the design idea of robot path planning and the path parameter selection method from the perspective of the spectrum. These approaches effectively reduce the flexible vibration of rotational motion.

In this study, the factors influencing the vibration behaviour of space robots were analysed, and the vibration of space robots was suppressed using the analysis results. First, the mechanical structure of the space robot was diagnosed, the integrated joint was assumed to be equivalent to a linear torsion spring, the flexible connecting rod was modelled by the finite element method, and the rigid-soft coupling dynamic model of the robot was established by combining the Lagrange method. The vibration model of the robot was obtained based on the dynamic model, and the vibration model was used to analyse the influence of the vibration force and frequency generated by the trajectory on the vibration, as well as the influence of different trajectories and loads on the natural frequency. Finally, vibration suppression was carried out using the trajectory planning method.

2. Rigid-Flexible Coupling Dynamic Model of Space Robots

2.1. Basic Composition. To improve the flexibility of the space robot, it had seven DOFs. The main characteristics of the robot are that it is lightweight and has a large load-weight ratio. The robot is equipped with a flexible integrated joint and lightweight connecting rod to satisfy the aforementioned characteristics. Figure 1 shows the configuration of the space robot SHIR5. The system mainly includes a mechanical system, control system framework, and operating system. The robot body is composed of an integrated joint, lightweight connecting rod, control box, and an external instructor, as shown in Figure 2.

An integrated joint is an essential part of a robot that integrates servomotors, reducers, torque sensors, encoders, and actuators. The composition of the integrated joints is illustrated in Figure 3. A high-performance permanent-magnet torque motor and harmonic reducer with a high transmission ratio were adopted to achieve lightness and a large load-weight ratio. A position encoder was installed at the motor and output shaft ends to improve the positioning accuracy. A torque sensor was installed at the output shaft of the joint module to realise compliant motion control of the manipulator and safety of the human fusion operation. Other components include brakes and drive control boards.

Owing to the immense flexibility of the harmonic reducer and torque sensor in the lightweight connecting rod and

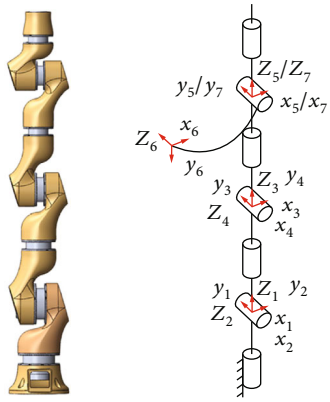

Figure 1: Configuration of space robot SHIR5.

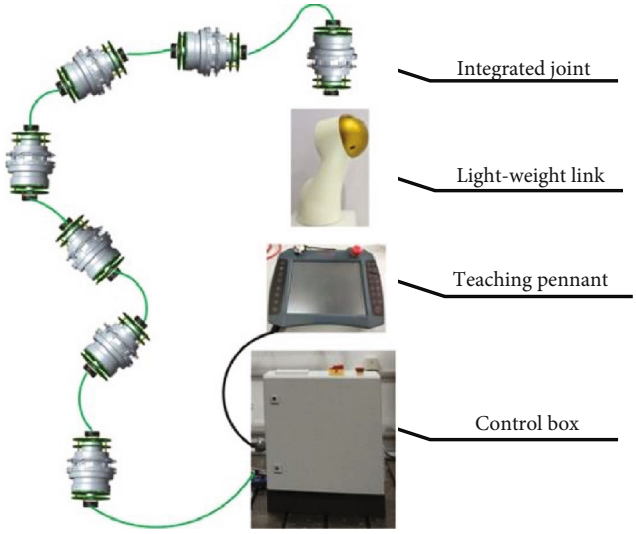

Figure 2: Composition of the robot system.

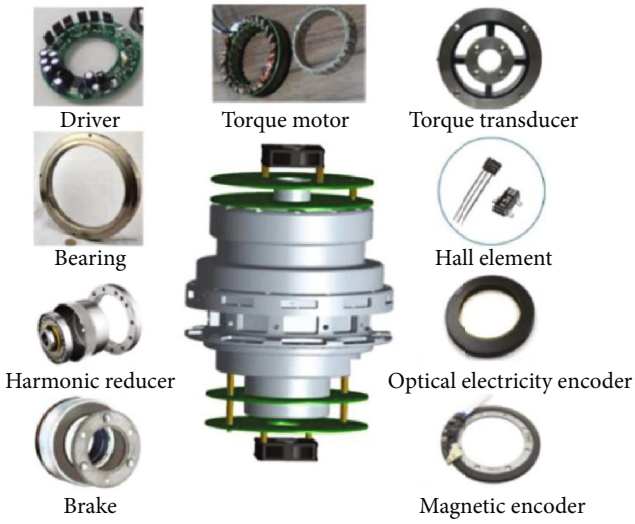

Figure 3: Composition of the integrative joints of robot.

integrated joint, the rigidity of the robot system is poor, which causes the robot to vibrate during operation and reduces its dynamic accuracy and stability. Hence, it was necessary to perform flexible coupling dynamic modelling and dynamic characteristic analysis of the robot.

2.2. Rigid-Flexible Coupling Dynamic Modelling. Figure 4(a) shows that the connecting rod of the robot was irregular in shape. First, the connecting rod was simplified and divided into circular, noncircular, and thin-walled parts. The noncircular thin-walled part was simplified through an elliptical section, which was conducive to establishing the solution model. A schematic of the thin circular and elliptical walls is shown in Figure 4(b). The diameter of the circular section was defined as D, and the major and minor axes of the elliptical section were defined as D and B, respectively. The minor axis of the ellipse was along the x-direction, and the thickness of the connecting rod was d.

The space robot is equipped with an integrated joint that uses a harmonic reducer and a torque sensor to increase joint flexibility. The tilting stiffness of the joint is significantly greater than its torsional stiffness. Therefore, this study simplified the joint using a linear torsional spring, as shown in Figure 5. θ is the rotation angle of the motor rotor obtained after conversion of the reduction ratio of the harmonic reducer. The motor rotor rotates the flexible rod using a harmonic reducer and torque sensor. k represents the stiffness of the joint and δ represents the elastic deformation of the joint.

An overall simplified model that considers the flexibility of the connecting rod and joint was obtained using the above simplification of the connecting rod and joint, and the robot was assembled. As shown in Figure 6, the connecting rod was simplified into two elements: a circular section and an elliptical section. The serial number of element j on connecting rod L_i was denoted by ij, and the length and mass per unit length of the element were denoted by l_{ij} and m_{ij}, respectively. The mass of joint J_i and the torsional stiffness were denoted by m_{pi} and k_i, respectively. Connecting rods L_7 and joint J_7 had little effect on the system. To simplify the model, L_7, J_7, and P were considered equivalent to a rigid connecting rod, a concentrated mass, and the load, respectively.

A spatial beam element was used to model the flexible link of the robot. The transverse bending deformation of the link was expressed by the cubic Hermite function. The axial tensile deformation and bending deformation around the axis were expressed by a linear function. The deformation displacement and deformation angle of the element were denoted as u and v, where $u = [u_x, u_y, u_z]^T$ and $v = [v_x, v_y, v_z]^T$, respectively. The flexible joint was simplified as a linear spring, and the flexible motion relationship of the robot was obtained.

A right-handed coordinate system was established for the robot. The base frame of the robot was $O - x_0y_0z_0$, and the local frame $O - x_iy_iz_i$ was fixed to the flexible link. The z-axis of the local frame always coincided with the axis of the i_{th} link, as shown in Figure 7. θ is the angle of the joint

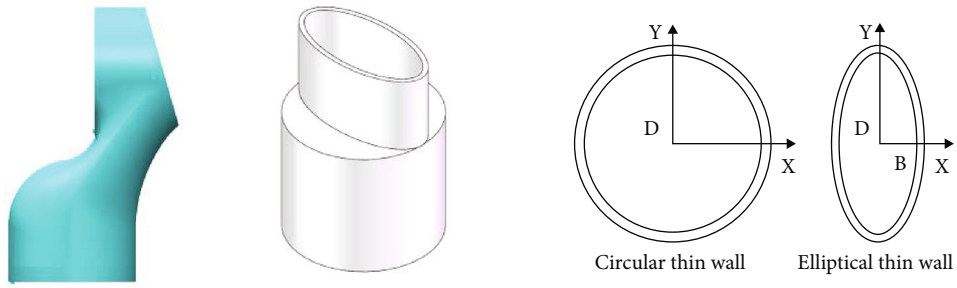

(a) Three-dimensional model and simplified model of the connecting rod (b) Thin-skin model

Figure 4: Simplified model of the connecting rod.

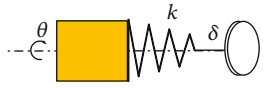

Figure 5: Simplified model of joints.

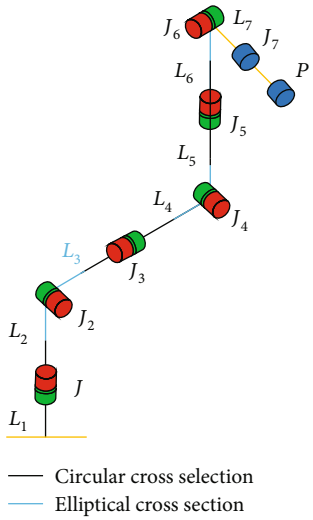

Figure 6: Simplified model of the joints.

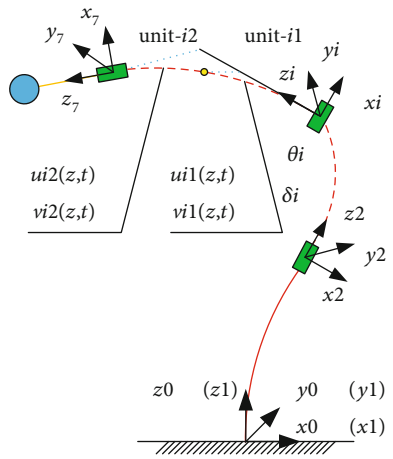

Figure 7: Flexible motion relationship of robot.

and δ is the flexible deformation of the joint. In a locally coordinated system, two units exist on the i_{th} link. In this study, the deflection and angle of unit deformation were represented by $u_{ij}(z,t)$ and $v_{ij}(z,t)$, respectively, where $i(i=1,2,\cdots,6)$ is the number of links, and $j(j=1,2)$ is the number of units, z is a point on the link unit.

It is assumed that $r_i{}'$ is the position of a point on the i_{th} link. When a point is located in the first unit of link, that is, when $j=1$, $r_i{}' = [u_{i1}(1,1), u_{i1}(2,1), \text{and}\, z + u_{i1}(3,1)]$ (1). When point is located in the second unit of link $(j=2)$, $r_i{}' = [u_{i2}(1,1), u_{i2}(2,1), \text{and}\, l_{i1} + z + u_{i2}(3,1)]$ (1). Thus, $r_i{}'$ can be described as

$$r_i' = \begin{bmatrix} 0 \\ 0 \\ (j-1)l_{i1} + z \\ 1 \end{bmatrix} + \begin{bmatrix} u_{ij} \\ 0 \end{bmatrix}, \tag{1}$$

where l_{i1} is the length of the first unit, $i=1,2,\cdots,6$, and $j=1,2$.

The transformation matrix of the flexible link can be obtained by multiplying the transformation matrix of the former link by that of the former joint. It is assumed that $T_{i1}=f_1(\theta)$, $T_{i2}=f_2(\delta)$, and $T_{i3}=f_3(u,v)$ are the transformation matrices of the joint revolution, flexible deformation of the joint, and the link, respectively.

When i is odd,

$$T_{i1} = \begin{bmatrix} \cos\theta_i & -\sin\theta_i & 0 & 0 \\ \sin\theta_i & \cos\theta_i & 0 & 0 \\ 0 & 0 & 1 & 0 \\ 0 & 0 & 0 & 1 \end{bmatrix},$$
$$T_{i2} = \begin{bmatrix} 1 & -\delta_i & 0 & 0 \\ \delta_i & 1 & 0 & 0 \\ 0 & 0 & 1 & 0 \\ 0 & 0 & 0 & 1 \end{bmatrix}. \tag{2}$$

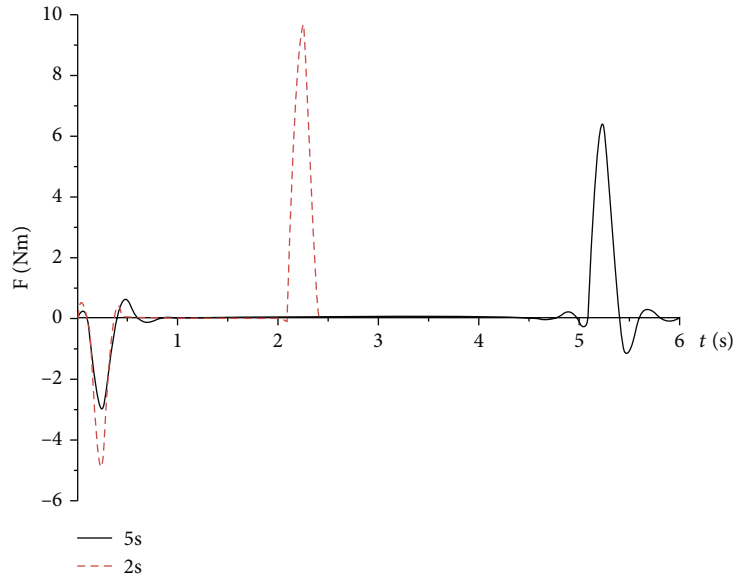

Figure 8: Excitation forces when task was completed in 5 s and 2 s.

When i is even,

$$T_{i1} = \begin{bmatrix} 1 & 0 & -\sin\theta_i & 0 \\ 0 & \cos\theta_i & 0 & 0 \\ 0 & \sin\theta_i & \cos\theta_i & 0 \\ 0 & 0 & 0 & 1 \end{bmatrix},$$

$$T_{i2} = \begin{bmatrix} 1 & 0 & 0 & 0 \\ 0 & 1 & -\delta_i & 0 \\ 0 & \delta_i & 1 & 0 \\ 0 & 0 & 0 & 1 \end{bmatrix}, \quad (3)$$

$$T_{i3} = \begin{bmatrix} 1 & -v_x & v_y & u_x \\ v_x & 1 & -v_z & u_y \\ -v_y & v_z & 1 & z+u_z \\ 0 & 0 & 0 & 1 \end{bmatrix}.$$

The position of any point on link i with respect to the base frame can be expressed as

$$r_i = T_{13} * T_{11} * T_{12} \cdots * T_{i3} * T_{i1} * T_{i2} * r_i'. \quad (4)$$

The velocity at any point on link can be obtained by calculating the derivative of r_i with respect to time. Then, the equations of the rigid-flexible coupled dynamics of the robot can be constructed based on the Lagrange formulation. In this study, the effects of the elastic deformation φ on the mass, damping, stiffness, and gravity matrices were ignored to simplify the dynamic model of the robot. Moreover, the H matrix was omitted because the centripetal and Coriolis forces have little influence on the dynamics. Thus, the dynamics of the robot can be expressed as

$$\begin{bmatrix} M_{\theta\theta}(\theta) & M_{\theta\varphi}(\theta) \\ M_{\theta\varphi}^T(\theta) & M_{\varphi\varphi}(\theta) \end{bmatrix} \begin{bmatrix} \ddot{\theta} \\ \ddot{\varphi} \end{bmatrix} + \begin{bmatrix} C_{\theta\theta}(\theta) & C_{\theta\varphi}(\theta) \\ C_{\theta\varphi}(\theta) & C_{\varphi\varphi}(\theta) \end{bmatrix} \begin{bmatrix} \dot{\theta} \\ \dot{\varphi} \end{bmatrix} + \begin{bmatrix} 0 & 0 \\ 0 & K(\theta) \end{bmatrix} \begin{bmatrix} \theta \\ \varphi \end{bmatrix} + \begin{bmatrix} G(\theta) \\ 0 \end{bmatrix} = \begin{bmatrix} \tau \\ 0 \end{bmatrix}, \quad (5)$$

where M, C, K, and G are the mass matrix, centripetal force, Coriolis force, stiffness matrix, and gravity of the system, respectively, and $\varphi = [\delta, u, v]$, τ is the torque required for the joint.

There are many ways to express the dynamic characteristics of robots. Natural frequency, as an essential indicator, can reflect the dynamic characteristics of a robot and its overall flexibility. The joint stiffness of the robot, structural parameters of the connecting rod, and load significantly influence the natural frequency of the robot, thereby affecting its dynamic characteristics. The natural frequency equation of the robot can be obtained using its dynamic model.

$$\det\left(\omega[I] - M^{-1}K\right) = 0. \quad (6)$$

3. Vibration Characteristics Analysis

Equation (5) can be rewritten as

$$M_{\varphi\varphi}(\theta)\ddot{\varphi} + C_{\varphi\varphi}(\theta)\dot{\varphi} + K(\theta)\varphi = -M_{\theta\varphi}^T(\theta)\ddot{\theta} - C_{\theta\varphi}^T(\theta)\dot{\theta}. \quad (7)$$

Equation (6) can be regarded as the vibration equation for the flexible deformation of a robot. The right side of the equation represents the excitation force. Thus, the equation of motion is obtained as follows:

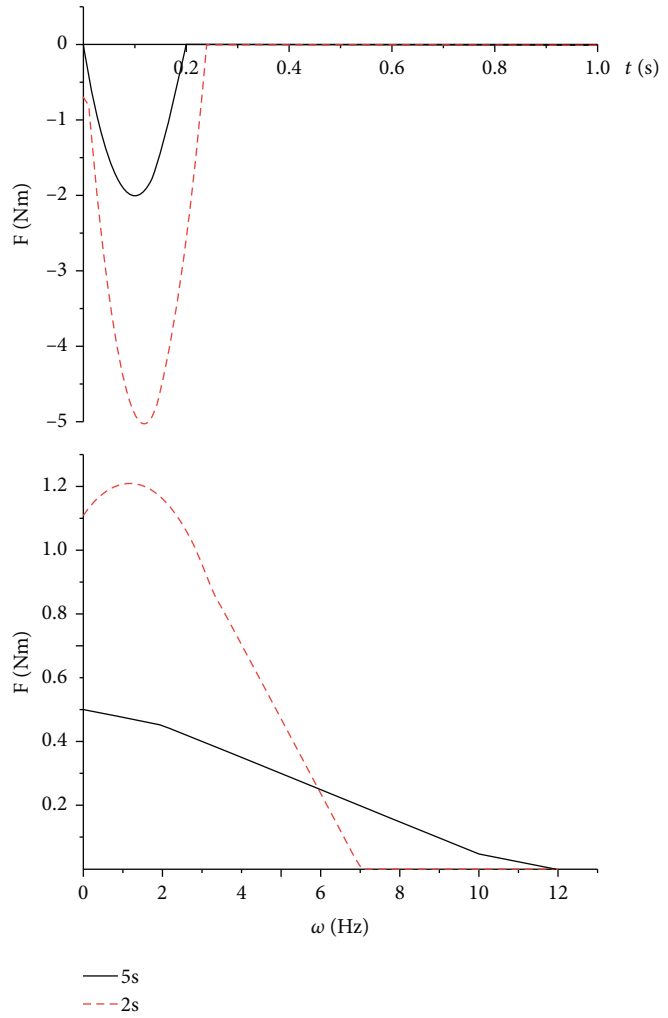

Figure 9: Frequency analysis of the excitation forces for tasks with different durations.

$$M_{\varphi\varphi}(\theta)\ddot{\varphi} + C_{\varphi\varphi}(\theta)\dot{\varphi} + K_{\varphi\varphi}\varphi = F\left(\theta, \dot{\theta}, \ddot{\theta}\right), \tag{8}$$

where $M_{\varphi\varphi}$, $C_{\varphi\varphi}$, $K_{\varphi\varphi}$, θ, φ, and F are the mass matrix, damping matrix, stiffness matrix, desired trajectory of the joint, flexible deformation of the link and joint, and excitation force, respectively, which are determined by the robot's desired motion.

The vibration response of a system can be classified as a transient or steady-state response. An effective method for suppressing the vibration of the robot is reducing the excitation force, because the steady response depends on the excitation force, which suppresses the vibration of the robot.

There are two types of vibrations in a robot: vibration during movement and residual vibration after movement. The steady-state response is the vibration generated by an external excitation force in the robot. The amplitude of the vibration was related to the magnitude and frequency of the excitation force. Resonance occurs when the frequency of the excitation force approaches the natural frequency.

Using a Fourier transform, the excitation force was decomposed into a series of simple harmonic excitation forces of different frequencies, and then a response superposition was performed. The steady-state response can be expressed as follows:

$$\begin{gathered} x(t) = B\sin(\omega t - \varphi), \\ B = \frac{F_0}{\sqrt{(k - m\omega^2)^2 + c^2\omega^2}} = \frac{F_0/k}{\sqrt{(1 - \nu^2)^2 + (2\xi\nu)^2}}, \\ \varphi = tg^{-1}\frac{c\omega}{k - m\omega^2} = tg^{-1}\frac{2\xi\nu}{1 - \nu^2}, \end{gathered} \tag{9}$$

where $\nu = \omega/\omega_n$ is the frequency ratio and $\xi = c/2\omega_n m$ is the damping ratio.

Therefore, when analysing the motion characteristics of a robot, the magnitude of the excitation force cannot be analysed, and the frequency must be analysed. The vibration equation of the robot shows that its elastic deformation varies with the rigid joint motion θ. This section discusses the dynamic characteristics of robots covering the same trajectories with durations of 2 and 5 s.

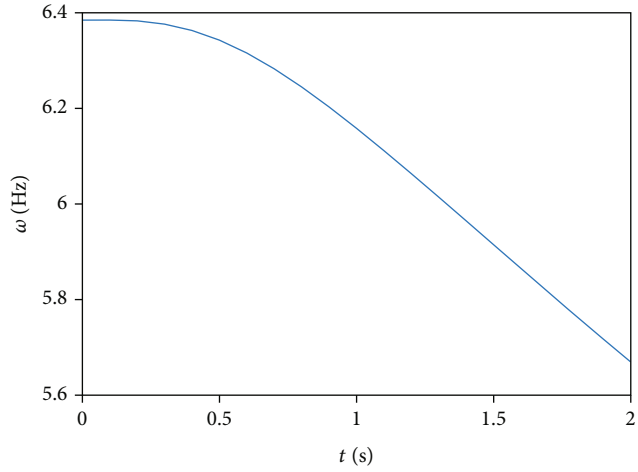

Figure 10: Change in the first-order natural frequency of the robot with respect to time.

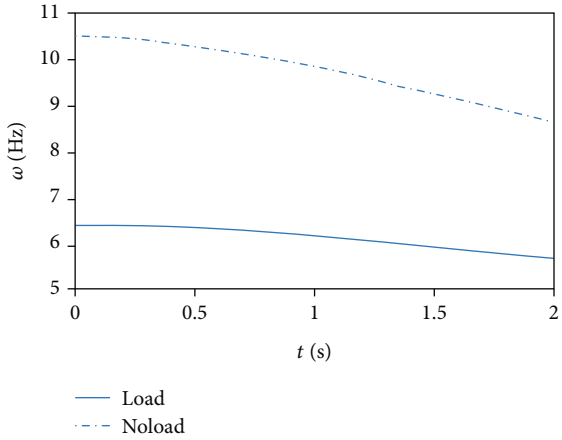

Figure 11: Effect of a load on the first-order natural frequency of the robot.

3.1. Influence of the Excitation Force on the Dynamic Characteristics of the Robot. When tasks with the same trajectory and different durations were completed, the excitation force F, which causes robot vibration, was found to differ with the duration of the trajectory. As shown in Figure 8, the excitation force F for the task completed in 5 s was smaller than that for the task completed in 2 s. Therefore, at the start and stop stages, the vibration of the robot when the task was completed in 2 s was more evident because of the larger excitation force F.

3.2. Influence of the Frequency on the Dynamic Characteristics of the Robot. The vibration amplitude of the robot is related to the magnitude of the excitation force, F, and its frequency. When the frequency of the excitation force was closer to the natural frequency of the system, the vibration became more intense. Therefore, it was necessary to analyse the frequencies of the excitation forces F_5 and F_2 for tasks having durations of 5 and 2 s. The results of the analysis are shown in Figure 9. The excitation frequency generated by the excitation force F_5 in the 5 s process is mainly distributed in the range of 0-10 Hz, and the excitation frequency generated by the excitation force F_2 in the 2 s process is primarily distributed in the range of 0-6 Hz. The excitation frequency generated by the excitation force F_2 in the process of 2 s is relatively concentrated. Therefore, the frequency of excitation force generated by different trajectories is different, thus affecting the excitation effect of the system.

As shown in Figure 10, the first-order natural frequency was between 5.7 and 6.4 Hz. Spectrum analysis of the excitation force (Figure 9) revealed that the amplitude of the frequency components in F_5 was higher than that in F_2. Therefore, during the subsequent relatively stable motion, the vibration generated when the task was completed in 5 s was more evident than that generated by the task with a 2 s duration when the excitation force was not significantly different.

3.3. Effect of a Load on the Dynamic Characteristics of the Robot. Figure 11 shows the change in the first-order natural frequency when the robot moved with and without a load. It can be observed that a load has a significant influence on the natural frequency. After adding the load, the natural frequency of the robot reduced, and the amplitude of the frequency components with similar excitation and natural frequencies increased; hence, the vibration intensified significantly. Therefore, the load cannot exceed a specific value to ensure dynamic accuracy and prevent severe vibration.

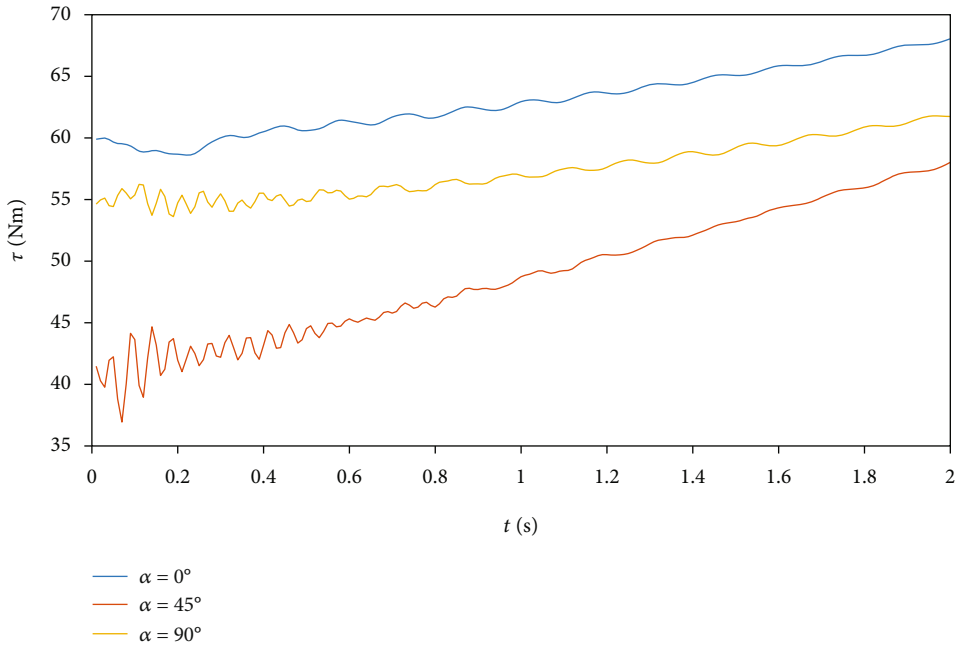

Figure 12: Effect of different initial arm angles on vibration of the robot.

Table 1: Initial value of arm angle corresponding to the angle of each joint.

α	0°	45°	90°
Joint angles	[-0.1484, 0.2176, 0, 1.7526, -0.3814, -0.4852, -0.1630]	[-1.1881, 0.6817, 1.4924, 1.7526, 0.3604, -0.4772, -1.5397]	[-1.0822, 1.2726, 1.9487, 1.7526, 0.6073, -0.7833, -2.4546]

3.4. Influence of the Initial Pose on Vibration. During the optimization process, the initial value of the arm angle α had a significant influence on the optimization results. For the same end position, different α values led to different initial joint angles and vibration effects. In this section, the effect of the initial arm angles on the end vibrations under the same trajectory is reported. The considered arm angles were 0°, 45°, and 90°. As shown in Figure 12, when the initial arm angle α was 0°, the torque of the joint was the largest, whereas the corresponding vibration was the smallest. When $\alpha = 45°$, the initial torque of the joint was the smallest; however, the corresponding vibration was significant. The angles of each joint of the robot corresponding to the initial arm angle α are listed in Table 1. In this study, when the initial conditions were relatively poor (i.e., $\alpha = 45°$), the initial vibration of the joint was significant.

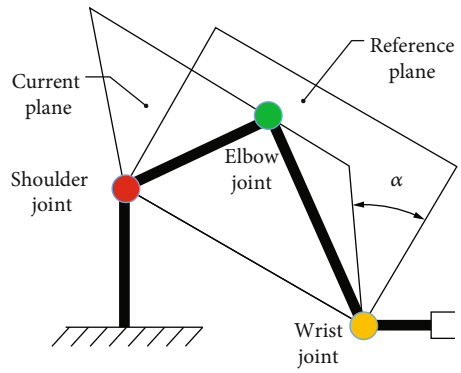

Figure 13: Principle diagram of the inverse kinematics solution for 7-DOF redundant robot.

4. Vibration Suppression

To ensure end accuracy, the arm angle of the robot was optimised in zero space using the analytical solution method, and a trajectory with a vibration suppression effect was obtained under the premise of satisfactory joint angle, angular velocity, and angular acceleration of the robot. The analytical solution method for the inverse solution of 7-DOF redundant robots is based on the method introduced [31], and its principle is illustrated in Figure 13. The shoulder and wrist joints are equivalent joints, and α is the arm angle, i.e., the angle between the current plane formed by the manipulator and the specified reference plane. Each joint angle value as a function of pose x and arm angle α is expressed as follows:

$$\theta = f^{-1}(x, \cdot \alpha), \tag{10}$$

where f denotes the kinematic function of the robot.

(a) Position and posture of P_1 (b) Position and posture of P_2

Figure 14: Initial posture and end posture of the robot.

The inverse kinematics solution method revealed that the robot's inverse kinematics were greatly affected by the angle α, which needs to be optimised in the solution process. The angular velocity of the joint and the angular velocity of the robot can be obtained by differentiating the joint angle of the robot as follows:

$$\begin{aligned} \dot{\theta}_{t+1} &= (\theta_{t+1} - \theta_t)/\Delta t, \\ \ddot{\theta}_{t+1} &= \left(\dot{\theta}_{t+1} - \dot{\theta}_t\right)/\Delta t, \end{aligned} \tag{11}$$

where Δt is one control cycle of the robot.

Using the above equations, the planning problem of the positioning layer was transformed into a problem of optimising the arm angle α for the minimum excitation force under the premise of a satisfactory joint angle, angular velocity, and angular acceleration.

$$\begin{aligned} \min \quad & \zeta = \left(M_{\theta\varphi}^T \ddot{\theta} + C_{\theta\varphi}^T \dot{\theta}\right)^T \left(M_{\theta\varphi}^T \ddot{\theta} + C_{\theta\varphi}^T \dot{\theta}\right), \\ \text{s.t.} \quad & \theta_{\min} \le \theta \le \theta_{\max}, \\ & V_{\min} \le \dot{\theta} \le V_{\max}, \\ & A_{\min} \le \ddot{\theta} \le A_{\max}. \end{aligned} \tag{12}$$

5. Experimental Study

An experimental study was conducted to validate the proposed vibration suppression method based on trajectory generation. Figure 14 shows a self-developed collaborative robot with seven DOFs and anthropomorphic configuration. The trajectory of the robot end was generated to study the impact of joint angle θ on the vibration of the robot. The robot end moved in a straight line from point P_1 to point P_2 and its attitude remained unchanged. The trajectory generation method is based on S-curve. The results for position, speed, maximum acceleration, and acceleration are shown in Figure 15. The details of the model parameters are listed in Table 2. The initial and target attitudes of the robot are shown in Figure 14. Planning parameters of the robot end are listed in Table 3.

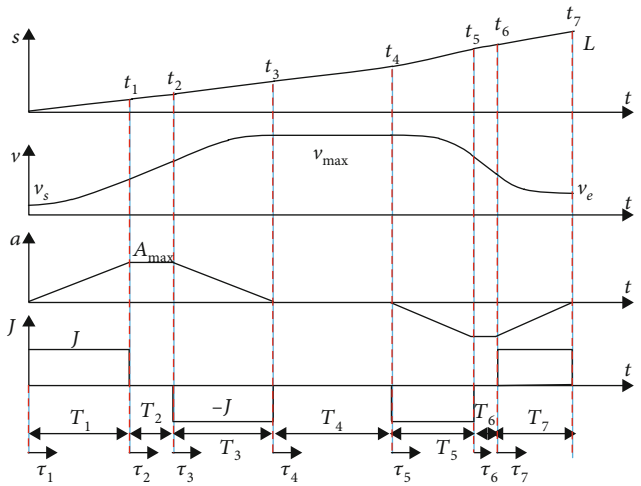

Figure 15: S-curve planning.

A torque sensor was mounted on the joint to measure the vibration of the robot. A low-pass filter was used to remove unwanted noise from the output of the torque sensor, and the amplitude of the signal was regarded as the amplitude of the vibration. The torque at the joint was calculated by substituting the actual angular velocity of the joint into the theoretical model.

v_{max} is the maximum speed of the robot end, T_k is the running time for each stage where $k = 1, 2, \cdots, 7$, L is the displacement of the robot throughout the operation, A_{max} is the maximum acceleration in the acceleration stage, and J is the acceleration of each stage.

5.1. Effects of Different Trajectories and Loads on Vibration. Torque sensors were used on the joints to observe the vibrations of the robot. Figure 16 shows the vibration behaviour of the robot that covers the same trajectory in 2 and 5 s. Initially, the vibration corresponding to the 2 s motion was significantly more intense than that corresponding to the 5 s motion. For subsequent motions, the vibration for the 5 s

Table 2: Initial posture and joint angle of the robot.

Points	P_1	P_2
Position/mm (x, y, z)	[506.102, -75.6716, 264.402]	[661.72, 370.513, 138.943]
Attitude/°	[1.5096, 86.8577, -29.4258]	[1.5096, 86.8577, -29.4258]
Joint angle/rad	[-0.1484, 0.2176, 0, 1.7526, -0.3814, -0.4852, -0.1630]	[0.5087, 0.8476, 0.0033, 1.0840, 0.8939, -0.6359, -1.3373]

Table 3: Planning parameters of the robot end.

Parameters	2 s	5 s
T_i/s	[0.08, 0, 0.08, 1.84, 0.08, 0, 0.08]	[0.18, 0, 0.18, 4.84, 0.18, 0, 0.18]
J/(mm/s^3)	[12260, 80460, -9930]	[1000, 2870, -920]
A/(mm/s^2)	[980, 6440, -800]	[180, 1150, -324]
v/(mm/s)	[78.5, 225.5, -64]	[31.5, 90.5, -25.5]
L/mm	[158, 454, -128]	[158, 454, -128]

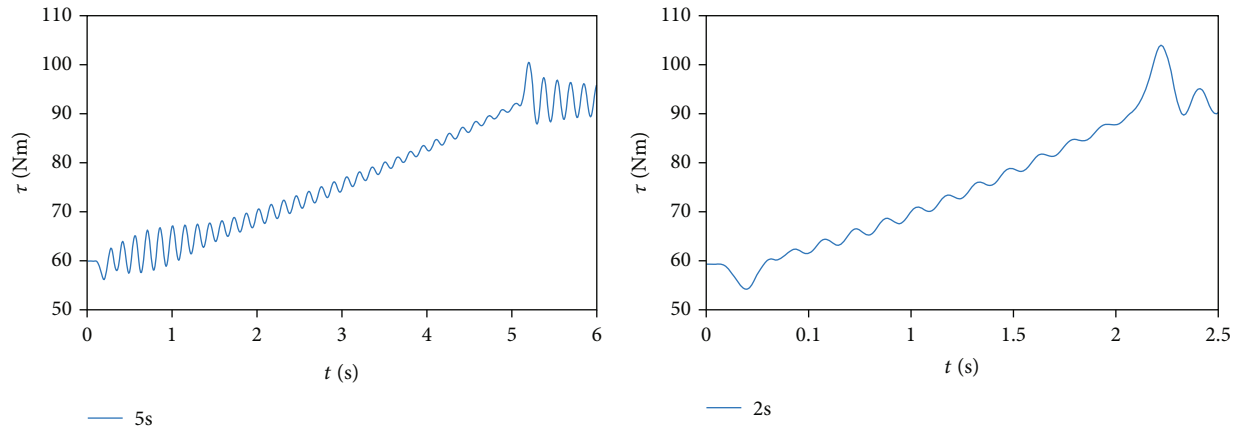

(a) Joint torque for the 5 s motion

(b) Joint torque for the 2 s motion

Figure 16: Influence of different trajectories on robot vibration.

motion was more intense than that for the 2 s motion. The excitation force F_2 was larger than F_5, indicating that the size of the excitation force alone did not determine the vibration of the robot.

It can be observed from the analysis results in Figure 17 that the load has a significant influence on the vibration of the robot. Its influence on the 2 s motion was smaller than that on the 5 s motion. With a load, the vibration for the 5 s motion was more pronounced; however, without a load, the vibration for the 5 s motion was significantly reduced. This reduction was more evident than that for the 2 s motion.

It can be observed from the vibration equation and vibration phenomenon of the robot that the trajectory of the robot joint has a significant influence on the excitation force. Therefore, the excitation force can be optimised by optimising the robot joint trajectory. The smaller the excitation force, the better the vibration reduction of the robot. For a task with a required end trajectory, the trajectory of the joint cannot be represented by the existing trajectory equation. Under the premise of a limited end trajectory, the redundant characteristics of the robot were used to optimise the joint trajectory through self-motion. Finally, vibration suppression of the robot was realised.

5.2. Verification of the Vibration Suppression Algorithm. For the results presented in this section, the initial arm angle α of the robot was set to 45°, the planning period of the robot was 0.01 s, and the robot load was 5 kg. The trajectory of the robot was optimised by the method described in this article. Then, the optimised robot joint trajectory was substituted into the dynamic model of the robot, and the torque of the second joint of the robot was obtained using the Newmark method.

Figure 18 shows the joint torque obtained by the position layer trajectory planning compared with that obtained before planning. Before vibration suppression, the robot experiences a slight vibration owing to the influence of

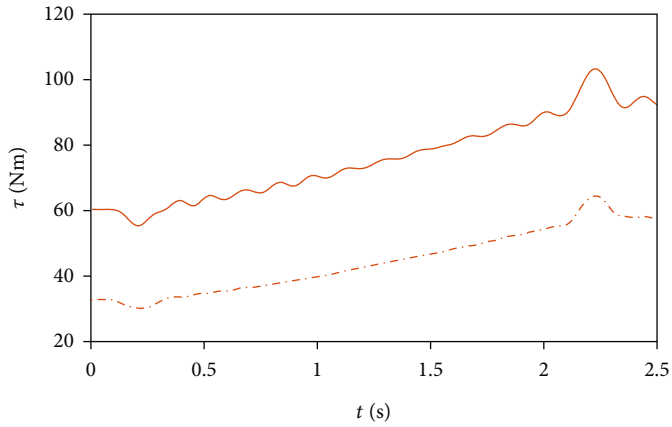

(a) Experimental data for the 2 s motion

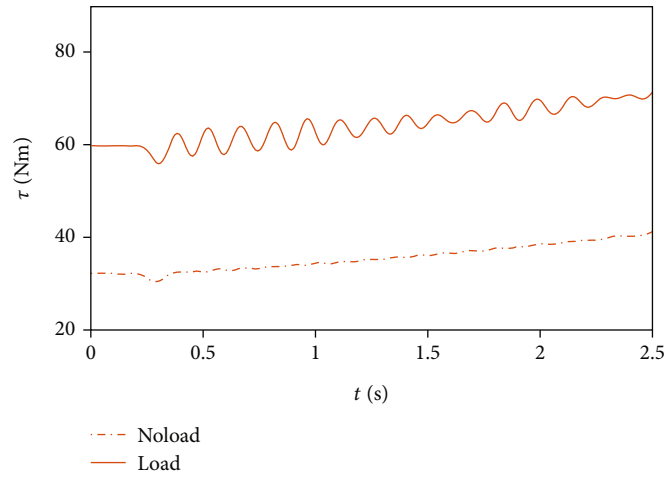

(b) Experimental data for the 5 s motion

Figure 17: Effect of the load on vibration.

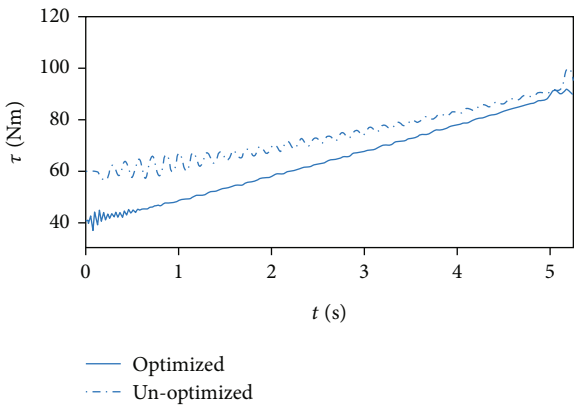

Figure 18: Comparison of joint torques before and after optimization.

acceleration during the initial movement, and the joint torque vibration amplitude is approximately 5 Nm. Subsequently, the vibration gradually becomes intense during smooth operation (0.5 s–1.5 s). The initial motion generates a shock force through the optimised trajectory owing to acceleration, resulting in a slight vibration, which is significantly weakened during smooth operation. Through comparison, the vibration of the joint torque after planning was considerably lower than that before planning, which illustrates the effectiveness of the trajectory planning method for vibration suppression of the robot.

Figure 19 compares the joint angles before and after the optimization of robot trajectory planning. It can be seen from the figure that the trajectory of optimised anterior and posterior joints 4 does not change. The trajectory of the other joints changes owing to the self-motion characteristics of the redundant robot.

Figure 20 shows the x-direction trajectory of the optimised front and rear ends. It can be seen from the figure that the trajectories of the front and back ends of the optimization are the same, indicating that the position layer trajectory planning can effectively suppress vibrations to ensure the end trajectory.

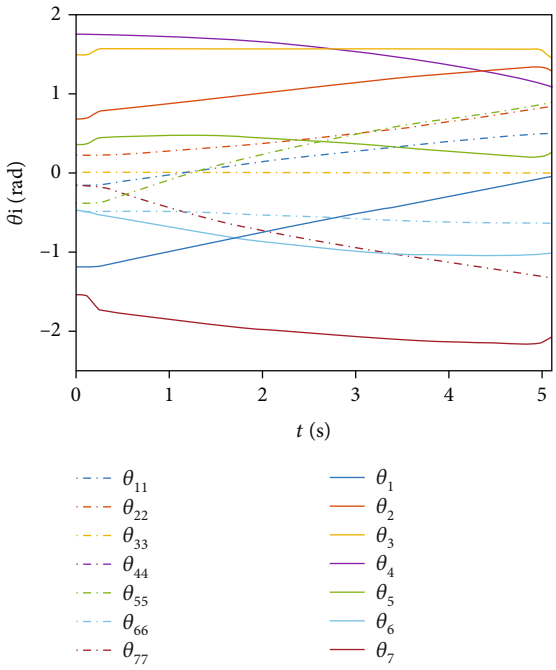

Figure 19: Contrast of joint trajectories. Note that θ_{ii} represents the unoptimised joint trajectory, and θ_i represents the optimised joint trajectory.

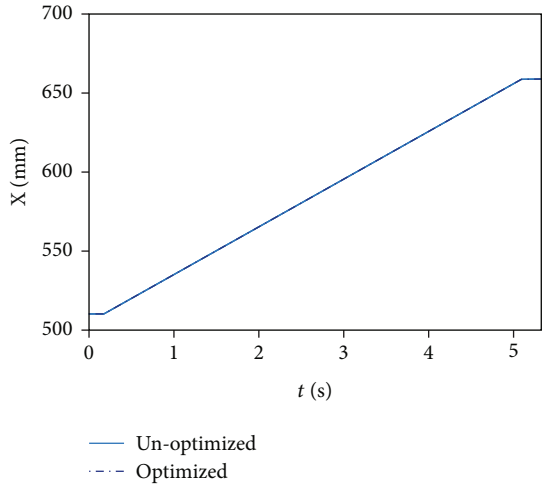

Figure 20: Trajectory of the robot end based on location planning.

6. Conclusions

In this study, the factors influencing the vibration behaviour of a robot were analysed by establishing a rigid-flexible coupling dynamic model of a flexible space robot. The following conclusions can be drawn: (1) the same path and different motion times lead to different vibration behaviours of the robot. In the trajectory planning process, the size and frequency of the excitation force should be considered comprehensively. The excitation force must be reduced and monitored to avoid the natural frequency of the system. (2) The loads affected the dynamic parameters of the robot and changed its natural frequency. Thus, the load capacity should be effectively limited during robot design. The above conclusions reveal the factors influencing robot vibration behaviour and provide support for the design and development of robots.

Subsequently, through the above analysis, the trajectory planning method was used to suppress the vibration of the robot, and the joint torque before and after the vibration suppression was compared experimentally. The vibration of the joint torque after planning was significantly lower than that before planning. The vibration amplitude reduced by 80%, which can improve the positioning accuracy and work efficiency of the robot, and illustrates the effectiveness of the trajectory planning method for the vibration suppression of a robot.

Data Availability

Data is available at http://www.re3data.org.

Conflicts of Interest

The authors declared no potential conflicts of interest with respect to the research, authorship, and/or publication of this article.

Acknowledgments

This work was supported in part by the National Natural Science Foundation of China under grant 51605311 and the Youth Program of Liaoning Education Department under grant LSNQN202025.

References

[1] H. Liu, D. Y. Liu, and Z. N. Jiang, "Space manipulator technology: review and prospect," *Acta Aeronauticaet Astronautica Sinica*, vol. 4, no. 1, pp. 524164–524164, 2021.

[2] G. Meng, L. L. Han, and C. F. Zhang, "Research progress and technical challenges of space robot," *Acta Aeronauticaet Astronautica Sinica*, vol. 42, no. 1, pp. 523963–523963, 2021.

[3] X. Zhang, J. G. Liu, J. Feng, Y. W. Liu, and Z. Ju, "Effective capture of nongraspable objects for space robots using geometric cage pairs," *IEEE/ASME Transactions on Mechatronics*, vol. 25, no. 1, pp. 95–107, 2019.

[4] X. Zhang, J. Liu, Y. Tong, Y. Liu, and Z. Ju, "Attitude decoupling control of semifloating space robots using time-delay estimation and supertwisting control," *IEEE Transactions on Aerospace Electronic Systems*, vol. 57, no. 6, pp. 4280–4295, 2021.

[5] X. Zhang and J. Liu, "Effective motion planning strategy for space robot capturing targets under consideration of the berth position," *Acta Astronautica*, vol. 148, pp. 403–416, 2018.

[6] H. Liu, D.-Y. Liu, and Z.-N. Jiang, "Review of space manipulator control technologies," *Robot*, vol. 44, no. 3, p. 22, 2022.

[7] M. Hu, H. Wang, and X. Pan, "Optimal configuration selection for stiffness identification of 7-Dof collaborative robots," *Intelligent Service Robotics*, vol. 13, no. 3, pp. 379–391, 2020.

[8] M. Hu, H. Wang, and X. Pan, "Multi-objective global optimum design of collaborative robots," *Structural Multidisciplinary Optimization*, vol. 62, no. 3, pp. 1547–1561, 2020.

[9] H. Liu, Z.-Q. Li, Y.-W. Liu et al., "Key technologies of TianGong-2 robotic hand and its on-orbit experiments," *Scientia Sinica Technologica*, vol. 48, no. 12, pp. 1313–1320, 2018.

[10] Z.-C. Qiu, "Review on research progress in vibration measurement and control of flexible manipulators," *Information and Control*, vol. 50, no. 2, p. 141, 2021.

[11] D. Bandopadhya, D. K. Bhogadi, B. Bhattacharya, and A. Dutta, "Active vibration suppression of a flexible link using ionic polymer metal composite," in *IEEE Conference on Robotics, Automation and Mechatronics*, pp. 1–6, Bangkok, Thailand, June 2006.

[12] A. Warkentin and S. E. Semercigil, "Variable stiffness control of a single-link flexible robotic arm," *Journal of Sound Vibration*, vol. 187, no. 1, pp. 1–21, 1995.

[13] L. Xie, X. Yu, and L. Chen, "Robust fuzzy sliding mode control and vibration suppression of free-floating flexible-link and flexible-joints space manipulator with external interference and uncertain parameter," *Robotica*, vol. 40, no. 4, pp. 997–1019, 2022.

[14] L. Sun, W. Yin, M. Wang, and J. Liu, "Position control for flexible joint robot based on online gravity compensation with vibration suppression," *IEEE Transactions on Industrial Electronics*, vol. 65, no. 6, pp. 4840–4848, 2017.

[15] K. Li, H. Wang, X. Liang, and Y. Miao, "Visual servoing of flexible-link manipulators by considering vibration suppression without deformation measurements," *IEEE Transactions on Cybernetics*, vol. 2021, pp. 1–10, 2021.

[16] M. P. P. Reddy and J. Jacob, "Vibration control of flexible link manipulator using SDRE controller and Kalman filtering," *Studies in Informatics and Control*, vol. 26, no. 2, pp. 143–150, 2017.

[17] H. Huang, G. Tang, H. Chen, L. Han, and D. Xie, "Dynamic modeling and vibration suppression for two-link underwater flexible manipulators," *IEEE Access*, vol. 10, pp. 40181–40196, 2022.

[18] D. Meng, W. Lu, W. Xu et al., "Vibration suppression control of free-floating space robots with flexible appendages for autonomous target capturing," *Acta Astronautica*, vol. 151, pp. 904–918, 2018.

[19] H. Sun, S. Hou, Q. Li, and X. Tang, "Research on the configuration of cable-driven parallel robots for vibration suppression of spatial flexible structures," *Aerospace Science and Technology*, vol. 109, article 106434, 2021.

[20] H. Liu, X. Lai, and W. Wu, "Time-optimal and jerk-continuous trajectory planning for robot manipulators with kinematic constraints," *Robotics Computer-Integrated Manufacturing*, vol. 29, no. 2, pp. 309–317, 2013.

[21] L. Cui, H. Wang, and W. Chen, "Trajectory planning of a spatial flexible manipulator for vibration suppression," *Robotics Autonomous Systems*, vol. 123, article 103316, 2020.

[22] T. Zhang, M. Zhang, and Y. Zou, "Time-optimal and smooth trajectory planning for robot manipulators," *International Journal of Control, Automation, Systems*, vol. 19, no. 1, pp. 521–531, 2021.

[23] B. Cao, K. Sun, T. Li, Y. Gu, M. Jin, and H. Liu, "Trajectory modified in joint space for vibration suppression of manipulator," *IEEE Access*, vol. 6, pp. 57969–57980, 2018.

[24] M. Wu, J. Mei, Y. Zhao, and W. Niu, "Vibration reduction of delta robot based on trajectory planning," *Mechanism Machine Theory*, vol. 153, article 104004, 2020.

[25] R. H. Lei and L. Chen, "Finite-time tracking control and vibration suppression based on the concept of virtual control force for flexible two-link space robot," *Defence Technology*, vol. 17, no. 3, pp. 874–883, 2021.

[26] C. Jalendra, B. Rout, and A. Marathe, "Vision sensor based residual vibration suppression strategy of non-deformable object for robot-assisted assembly operation with gripper flexibility," *Industrial Robot: the international journal of robotics research and application*, vol. 49, no. 5, pp. 851–864, 2022.

[27] Y.-F. Du and C. Wang, "Residual vibration control of flexible manipulator," *Journal of Vibration and Shock*, vol. 38, no. 7, pp. 165–171, 2019.

[28] L. Zhao, "Dynamic analysis of a flexible robotic arm carrying a moving end effector," *Journal of Vibration and Shock*, vol. 39, no. 8, pp. 112–117, 2020.

[29] Z. Yu, Y. Guo, W. Yao, Y. F. Wu, and J. Guo, "Experiments on path planning for rotational motions of a flexible manipulator using spectral analysis based approach," *Journal of Vibration Engineering*, vol. 33, no. 4, pp. 717–723, 2020.

[30] Z. Yu, C. Zhong, and Y. Guo, "Spectral analysis and parameter selection for BCB attitude maneuver path of flexible spacecraft," in *IEEE International Conference on Information & Automation*, pp. 729–734, Yinchuan, China, August, 2013.

[31] M. Shimizu, H. Kakuya, W.-K. Yoon, K. Kitagaki, and K. Kosuge, "Analytical inverse kinematic computation for 7-DOF redundant manipulators with joint limits and its application to redundancy resolution," *IEEE Transactions on Robotics*, vol. 24, no. 5, pp. 1131–1142, 2008.